



ORIGINAL ARTICLE

Behavior of composite beams with external prestressing in sagging moment regions

Comportamento de vigas mistas com protensão externa nas regiões de momento positivo

Karla Demoner Ribeiro^a Thiago Tononi Turini^a Lorenzo Augusto Ruschi e Luchi^a Adenilcia Fernanda Groberio Calenzani^a ^aUniversidade Federal do Espírito Santo – UFES, Departamento de Engenharia Civil, Vitória, ES, Brasil

Received 08 October 2019

Accepted 14 December 2020

Abstract: Prestressed composite steel-concrete structures are scarcely used due to a lack of clear standardized design guidelines and formulations on the subject. The present research aims to present design methodologies for steel-concrete composite beams with external pretension applied via straight tendons. A computer program to perform structural analysis of such beams was developed based on two different methodologies: the first one is presented in ABNT NBR 8800:2008, in which the guidelines for the design of composite beams with compact webs are adjusted to include the effects of the pretension force. The second methodology is extracted from international literature and presents a structural design process based on stress distribution on the beam. Ninety prestressed and thirty non-prestressed beams were analyzed and designed with the aforementioned computer program to evaluate the influence of beam length, degree of symmetry of the steel profile and eccentricity of the pretension force on the mechanical resistance of the beams. It was observed that, although the prestressing force considerably improved resistance to bending, it introduced high compression stresses on the steel profile; hence, the pre-stressing of composite beams is proved efficient only for steel profiles with symmetrical cross-sections.

Keywords: prestressed composite beams. design methodology. external prestressing. computer program.

Resumo: A protensão em estruturas mistas de aço e concreto é pouco utilizada pela falta de normas e formulações claras sobre o assunto. Esse trabalho visa apresentar metodologias de análise e dimensionamento de vigas biapoiadas mistas de aço e concreto com protensão externa e cabo de traçado reto (pré-tração). Um programa computacional que efetua a análise e o dimensionamento dessas vigas foi elaborado com base em duas metodologias distintas: a da ABNT NBR 8800:2008, de vigas mistas compactas, ajustada para incluir os efeitos da força de protensão e uma segunda, extraída da literatura internacional, em que o dimensionamento é feito por meio da verificação das tensões atuantes. Noventa vigas mistas protendidas e trinta sem protensão foram calculadas por meio do programa computacional desenvolvido para avaliar a influência do comprimento do vão, do grau de monossimetria da seção transversal do perfil de aço e da excentricidade da força de protensão na capacidade resistente das vigas. Observou-se que embora a protensão gere uma melhora considerável no comportamento à flexão, a força de protensão introduz altas tensões de compressão no perfil de aço, por isso a eficiência da protensão foi comprovada apenas nos casos de vigas mistas com perfil de aço duplamente simétrico.

Palavras-chave: vigas mistas de aço e concreto protendidas. metodologias de dimensionamento. protensão externa. programa computacional.

How to cite: K. D. Ribeiro, T. T. Turini, L. A. R. Luchi, and A. F. G. Calenzani, “Behavior of composite beams with external prestressing in sagging moment regions,” *Rev. IBRACON Estrut. Mater.*, vol. 14, no. 4, e14405, 2021, <https://doi.org/10.1590/S1983-41952021000400005>

Corresponding author: Adenilcia Fernanda Groberio Calenzani. E-mail: afcalenzani@gmail.com

Financial support: Foundation for Support of Research and Innovation of Espírito Santo (FAPES), with a master’s scholarship of R\$1,500.00 monthly to Karla Demoner Ribeiro.

Conflict of interest: Nothing to declare.



This is an Open Access article distributed under the terms of the Creative Commons Attribution License, which permits unrestricted use, distribution, and reproduction in any medium, provided the original work is properly cited.

1 INTRODUCTION

External prestressing applied to steel-concrete composite beams results in elements of great structural efficiency, able to cover large spans and resist high loads with reduced structural weight. This technique is of interest for structural recovery and / or reinforcement of existing structures presenting severe pathologies caused by deterioration due to environmental agents or increases in service loads such as, for example, a bridge that experiences an increase in traffic or other loads throughout its lifespan.

Advantages of using external prestressing systems include: the absence of sheaths, which facilitates the building process, making construction more agile; possibility of reducing cross-sections, resulting in lighter and more efficient structural elements; reduction of prestressing losses due to friction, which may even be neglected when using unbonded tendons; external tendons with simpler lines and easier verification after installation; since tendons are external, they are easily inspected and can be re-prestressed or even replaced without interrupting the use of the structure. Figure 1 shows different cross-section types for composite beams with external prestressing tendons.

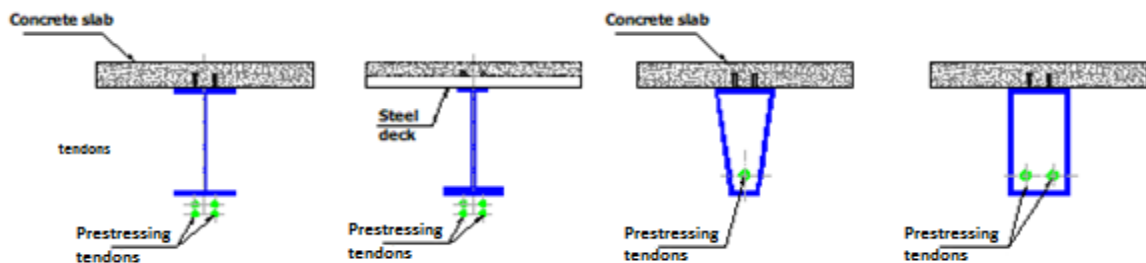


Figure 1. Possible profiles for external prestressing. Source: Troitsky [1].

Studies indicate that the application of prestressing to composite steel-concrete structures is recent. Ayyub et al. [2] and Troitsky [1] state that in 1959, Szilard [3] suggested methods for the analysis and design of prestressed composite steel-concrete beams considering the effects of concrete shrinkage and creep. Hoadley [4], in 1963, investigated the behavior of simply supported steel and steel-concrete composite beams, prestressed with high resistance tendons and constant eccentricity along the beam. Strass [5], in the following year, developed an experimental study of composite steel-concrete beams subjected to positive bending moment. In 1966, Regan [6] analyzed the effects of variations in slab thickness, prestressing forces and load types on the behavior of simply supported composite steel-concrete beams.

Saadatmanesh et al. [7] to [8] published a series of analytical and experimental studies on prestressed composite beams in the regions of sagging and hogging bending moments. The authors reported some of the advantages of using prestressing in composite beams such as: reductions in the weight of structural steel; increases in the range of the linear elastic regime of the structure; increased strength; and improvements in fatigue and fracture behavior.

Saadatmanesh et al. [9] tested two composite beams, one subjected to positive bending moment and the other to negative bending moment. The steel beams were prestressed before concrete casting to prevent cracking of the slab. Force versus displacement graphs of the beams were plotted, as well as graphs of force versus strain of the concrete, steel beam and prestressing bars. The values measured experimentally correlated well with values predicted by Saadatmanesh et al. [7], who used internal force equilibrium equations and strain compatibility.

Chen and Gu [10] experimentally determined the strength of sagging moment regions in prestressed composite steel-concrete beams. In the first stage, the beams were tested without prestressing until the bottom flange of the steel beam began yielding, at which point the beams were unloaded. In the second stage, prestressing was applied to the composite beams before loading. The methodology adopted made it possible to analyze the behavior of the composite beams without prestressing. Additionally, based on the deformation compatibility of the tendons and the beam in the anchoring section and by balancing internal forces, the equation of the neutral axis is derived. A simplified expression to determine increases of stress on the tendons is developed, according to the method used to evaluate the capacity of the prestressed composite beam.

In Brazil, among studies on the use of external prestressing in composite beams, one can mention Nelsen [11] and Linhares [12]. Nelsen [11] presented a systematic approach for the analytical design procedure of simply supported and externally prestressed composite steel-concrete I-beams based on requirements from ABNT NBR 8800: 2008 [13], with emphasis on ultimate limit states (ULS). The author studied the influence of prestress force levels, eccentricity of the

tendons and constructive methodology (pre-tensioning or post-tensioning) on the strength of structural elements, using spreadsheets developed with the software MathCAD.

Linhaires [12] carried out a case study of an externally prestressed composite box-girder bridge featuring two continuous spans, proceeding to an analytical verification following design criteria from AASHTO-LRFD. An initial model consisting of spatial frame bars was developed with the software STRAP for the structural analysis of the system, followed by the creation of a more refined finite element model featuring shell elements with the aid of the computer program SAP2000, to confront and validate the results of the initial model, especially in terms of stresses and displacements. The author concluded that prestressing the composite beam resulted in a small increase in flexural strength in the region subjected to positive bending moment, proving to be of little advantage, according to the AASHTO design criteria. The calculation of prestress force losses due to friction resulted in a small value, since the span only presented two inflection points.

Recently, Lou et al. [14] developed a FE model to analyze composite steel and concrete beams with external prestressing under short and long-term loads, aiming to compare results with composite steel and concrete beams without prestressing. The effect of geometric non-linearity was added by considering the flexural and axial interaction in the finite element formulation, updating the eccentricities of the tendons in the numerical procedure. Results confirmed that prestressing composite beams considerably improved their behavior under short loads. However, there was no noticeable difference on the response to time-dependent effects.

Liban and Tayşi [15], on the other hand, performed a numerical analysis of a simply supported pre-tensioned composite beam with overhangs, in order to observe the behavior of regions subjected to positive and negative bending moments, and also assess the influence of tendon position on the behavior of the structure. Results show that it is more beneficial for the structure to place the straight tendon near the top flange of the profile, thus obtaining an ultimate load approximately 22% larger than if the straight tendon was positioned near the bottom flange of the profile.

On this research, a computer program was developed using Microsoft Office Excel [16] with an interface in Visual Basic language, in the Microsoft Visual Basic Express environment [17]. The program performs the analysis and design of simply supported composite steel and concrete beams with external prestressing and straight tendons (pre-tension), checking safety conditions for ultimate limit states and the serviceability limit state (SLS) of excessive deflection.

1.1 Theoretical formulation

The Brazilian standard NBR 8800: 2008 [13] addresses the design of composite steel and concrete beams without prestressing. Thus, for this research, the design equations were adjusted to include the effects of prestressing forces. This force is estimated according to Nunziata [18], considering that the maximum compressive stress in the central section of the steel profile at the time of prestressing cannot exceed the design yield strength of steel, according to Equation 1.

$$\frac{M_g}{W_a} - \frac{P\beta_n\gamma_p}{A_a} - \frac{P\beta_n\gamma_p e_{p-a}}{W_a} = -f_{yd} \tag{1}$$

It is worth mentioning that at first, since the element is subjected to pre-tensioning with prestressing occurring before the application of the construction loads, the steel beam must resist all the stresses introduced by prestressing. As such, the formulation of Equation 1 uses the properties of the steel profile. Isolation of the prestressing force P results in Equation 2:

$$P = \frac{\frac{M_g}{W_a} + f_{yd}}{\frac{\beta_n\gamma_p}{A_a} + \frac{\beta_n\gamma_p e_{p-a}}{W_a}} \tag{2}$$

Where: P is the prestressing force, f_{yd} is the design yield strength of the steel of the profile, M_g is the maximum bending moment caused by the weight of the profile, W_a is the elastic section modulus of the steel profile, e_{p-a} is the eccentricity of the prestressing tendon in relation to the center of gravity of the steel cross-section, A_a is the cross-

sectional area of the steel profile, γ_p is a safety factor applied to the prestressing force and β_n is the amplification factor of the prestressing force, introduced to compensate for losses in prestress force, taken as 1.1.

Equation 2 was adjusted to fit the flexo-compression interaction curve of NBR 8800: 2008 [13]. Assuming that the design axial force is greater than 20% of the design resistance to axial force, Equation 3, the prestressing force value is obtained according to Equation 5. Furthermore, the term related to the bending moment due to the weight of the steel beam cannot be considered when the tendon layout is straight, since the effects favoring structural safety do not occur at the supported cross-sections in this case.

$$\frac{N_{Sd} + \frac{8M_{Sd}}{9M_{Rd}} \leq 1 \text{ to } \frac{N_{Sd}}{N_{Rd}} > 0.2 \tag{3}$$

$$\frac{\gamma_p \beta_n P}{N_{Rd}} + \frac{8\gamma_p \beta_n P e_{p-a}}{9M_{Rd}} \leq 1 \tag{4}$$

$$P = \frac{1}{\frac{\gamma_p \beta_n}{N_{Rd}} + \frac{8\gamma_p \beta_n e_{p-a}}{9M_{Rd}}} \tag{5}$$

where M_{Rd} is the design resistance to bending moment of the steel beam, γ_p is the load factor of prestressing force, N_{Rd} is the design resistance to axial force of the steel beam and e_{p-a} is the eccentricity of the tendon in relation to the centroid of the beam cross-section. Remaining variables are defined according to Equation 2.

With the application of the gravitational loads of construction, an increase in the value of the initial prestressing force is assumed, which varies according to the configuration of the prestressing tendon and the distribution of the load. This increase in the value of the initial prestressing force, called force increment, can be calculated in several ways, such as: with the application of the principle of virtual work (Troitsky [1]); deformation increment method or finite element method. If a straight tendon is considered, the expressions to determine the increase in prestressing force ΔP are Equation 6 for uniformly distributed load q and Equation 7 for two symmetrically placed concentrated loads F of same magnitude, at a distance a from supports.

$$\Delta P = \frac{qL^2 e_{p-tr}}{12 \left(e_{p-tr}^2 + \frac{I_{tr}}{A_{tr}} + \frac{E_a I_{tr}}{E_p A_p} \right)} \tag{6}$$

$$\Delta P = \frac{e_{p-tr} Fa(L-a)}{L \left(e_{p-tr}^2 + \frac{I_{tr}}{A_{tr}} + \frac{E_a I_{tr}}{E_p A_p} \right)} \tag{7}$$

where E_a is the modulus of elasticity of the steel profile, E_p is the modulus of elasticity of the prestressing tendon, L is the length of said tendon, equal to the length of the beam, I_{tr} is the moment of inertia of the composite section, A_p is the area of active reinforcing steel, A_{tr} is the area of the transformed composite section, e_{p-tr} is the eccentricity of the prestressing tendon in relation to the centroid of the composite section and q is the uniformly distributed load. Remaining variables are defined according to Equation 5.

1.2 Simplifying assumptions

The present study was limited to the verification of simply supported composite steel and concrete beams with external prestressing (pre-tension) in regions of positive moment. The steel section and the prestressed composite section were designed with procedures defined in the standards: ABNT NBR 8800: 2008 [13], ABNT NBR 6118: 2014

[19], ABNT NBR 7482: 2008 [20] and ABNT NBR 7483: 2008 [21]. Some premises that simplify the analysis and limit the scope of the study were adopted, namely:

- Compact steel section, that is, local flange or web buckling is not expected, meaning that $Q_a = Q_s = Q = 1$;
- Complete interaction between steel and concrete materials, guaranteed by the proper design of stud bolt shear connectors;
- Unshored construction;
- Solid reinforced-concrete slab;
- Tensile strength of concrete is neglected;
- Straight line tendon;
- Verification is limited to the mid-span section, where the largest bending moment is expected;
- Shear force is resisted only by the steel profile.

2 PRESENTATION OF THE PROGRAM

The program verifies the ultimate resistance to bending of the prestressed composite beam according to the methodology adopted by ABNT NBR 8800: 2008 [13] but with the modifications proposed in item 1.1 of this paper. Doubly and monosymmetric steel profiles are accepted by the program. There is also the option of using the procedure proposed by Nunziata [18], which checks the stresses on steel and concrete.

Design routines were developed in the form of flowcharts to systematize the entire script and assist in the elaboration of the program. The routines illustrate the procedures performed, clarifying the sequence of calculations, indicating the design equations used and the basic commands needed such as decision and data selection. In total, 11 routines were developed. Routine 1 calculates the position of the elastic neutral axis, ENA, and the moment of inertia of the homogenized composite section.

Routines 2 and 3 calculate the design resistance to compression and the design resistance to bending moment of the steel profile, respectively. Routines 4 and 5 are intended, respectively, for calculating the prestressing force and its increase. Routine 6 verifies the combined bending and axial stresses of the steel profile.

Routine 7 calculates the position of the plastic neutral axis, PNA, measured from the top of the slab, symbolized by the letter a when it passes through the slab and by y_{LNP} when it crosses the steel profile. This routine also provides an expression for the ultimate bending moment of the composite section.

Routine 8 calculates the ultimate shear force, routine 9 determines the midspan deflection of the prestressed composite section and in routine 10, the calculation of stresses on steel and concrete is presented. Finally, routine 11 includes the calculation of the number of shear connectors needed for full interaction. The complete flowcharts for routines 1 to 11 are presented in Ribeiro [22].

The logic used in the program, enumerated below, performs the design in three stages of the lifespan of the structure: phase 1, during construction, when the steel profile resists the construction loads and the prestressing force; phase 2, when composite behavior is developed and the composite beam supports immediate loads such as live loads attributed to occupation and finally phase 3, when long-term effects are considered. Table 1 shows the loads considered in the structural analysis and Table 2 shows the load factors according to ABNT NBR 8800: 2008 [13] for construction load combination (before curing) and for normal load combination (after curing). Applied loads are calculated using construction combinations in phase 1 and normal combinations in phases 2 and 3.

Table 1. Load considered in structural analysis

(1)	g_1 – Weight of the steel beam
(2)	P – Prestressing force on steel tendons
(3)	g_3 – Weight of the concrete slab
(4)	ΔP_4 - Increment of prestressing force due to the weight of the concrete slab
(5)	g_5 – Serviceability dead load
(6)	q_6 – Serviceability live load
(7)	ΔP_7 - - Increment of prestressing force due to serviceability dead load
(8)	ΔP_8 - - Increment of prestressing force due to serviceability live load
(9)	P_9 – Concrete slab shrinkage

Table 2. Loads safety factor (γ)

Loads	Before Concrete Casting	After Concrete Casting
Weight of the steel beam (g_1)	$\gamma'_{g1} = 1.15$	$\gamma_{g1} = 1.25$
Prestressing force on steel tendons (P)	$\gamma'_{g2} = 1.20$	$\gamma_{g2} = 1.20$
Weight of the concrete slab (g_3)	$\gamma'_{g3} = 1.25$	$\gamma_{g3} = 1.35$
Serviceability dead load (g_5)	-	$\gamma_{g5} = 1.35$
Serviceability live load (q_6)	-	$\gamma_{g6} = 1.50$

1) Data input, calculation of geometric properties and ultimate forces of the steel profile and calculation of prestressing force:

- Calculation of the geometric properties of the cross-section of the steel profile;
- Calculation of the PNA of the steel profile section;
- Calculation of the number of stud bolts;
- Call Routine 1 - Calculation of the ENA of the homogenized section;
- Call Routine 2 - Calculation of the design resistance to compression (N_{Rd}) of the steel profile;
- Call Routine 3 - Calculation of the design resistance to negative moment (M_{Rd}^-) of the steel profile;
- Call Routine 4 - Calculation of the initial prestressing force (P);

2) Design according to NBR 8800:2008 [13]:

2.1) Verification in phase 1 – Steel beam

- Loads: (1) + (2) + (3) + (4);
- Call Routine 5 - Calculation of increases in prestressing force (ΔP_4) due to the weight of the concrete slab and verification of maximum stress on the tendons after force increments;
- Calculation of the design compression force (N_{Sd_1}) of phase 1:

$$N_{Sd_1} = \gamma_{g2} \cdot \beta_n \cdot P + \gamma_{g2} \cdot \beta_n \cdot \Delta P_4 \tag{8}$$

- Calculation of the design bending moment (M_{Sd_1}) of phase 1:

$$M_{Sd_1} = \frac{\gamma'_{g1} \cdot g_1 \cdot L_v^2}{8} + \gamma_{g2} \cdot \beta_n \cdot P \cdot e_{p_a} + \frac{\gamma'_{g3} \cdot g_3 \cdot L_v^2}{8} + \gamma_{g2} \cdot \beta_n \cdot \Delta P_4 \cdot e_{p_a} \tag{9}$$

- Call routine 3 – Calculation of the resistance to bending of the steel profile, M_{Rd_1} , resistance to negative (M_{Rd}^-) or positive (M_{Rd}^+) bending moment, depending on the value of M_{Sd_1} ;
- Call routine 6 – Flexo-compression design:

$$\frac{N_{Sd_1}}{N_{Rd_1}} + \frac{8 \cdot M_{Sd_1}}{9 \cdot M_{Rd_1}} \leq 1 \tag{10}$$

- Calculation of the design shear force (V_{Sd_1}) of phase 1:

$$V_{Sd_1} = \frac{\gamma'_{g1} \cdot g_1 \cdot L_v}{2} + \frac{\gamma'_{g3} \cdot g_3 \cdot L_v}{2} \tag{11}$$

- Call routine 8 – Calculation of the design resistance to shear force (V_{Rd}) of the steel profile;
- Verification $V_{Sd_1} \leq V_{Rd}$;

2.2) Verification in phase 2 – Steel-concrete composite beam, $t=0$ and $n = \frac{E_a}{E_c}$

- Loads: (1) + (2) + (3) + (4) + (5) + (6) + (7) + (8);
- Call routine 5 – Calculation of increments in prestressing force due to applied loads. Calculates increments due to dead loads (ΔP_7) and live loads (ΔP_8) and verifies maximum stresses on the tendons after the increments;
- Calculation of the design axial force (N_{Sd_2}) in phase 2:

$$N_{Sd_2} = N_{Sd_1} + \gamma_{g2} \cdot \beta_n \cdot \Delta P_7 + \gamma_{g2} \cdot \beta_n \cdot \Delta P_8 \quad (12)$$

- Calculation of the design bending moment (M_{Sd_2}) of phase 2:

$$M_{Sd_2} = M_{Sd_1} + \frac{\gamma_{g5} \cdot g_5 \cdot L_v^2}{8} + \frac{\gamma_{g6} \cdot q_6 \cdot L_v^2}{8} + \gamma_{g2} \cdot \beta_n \cdot \Delta P_7 \cdot e_{p_tr} + \gamma_{g2} \cdot \beta_n \cdot \Delta P_8 \cdot e_{p_tr} \quad (13)$$

- Call routine 7 – Calculation of PNA and design resistance to bending moment (M_{Rd_2}) of the prestressed composite section;
- Call routine 6 – Flexo-Compression verification:

$$\frac{N_{Sd_2}}{N_{Rd}} + \frac{8 \cdot M_{Sd_2}}{9 \cdot M_{Rd_2}} \leq 1 \quad (14)$$

For simplification, it is assumed that only the steel profile resists axial forces.

- Calculation of the design shear force (V_{Sd_2}) of phase 2:

$$V_{Sd_2} = V_{Sd_1} + \frac{\gamma_{g5} \cdot g_5 \cdot L_v}{2} + \frac{\gamma_{g6} \cdot q_6 \cdot L_v}{2} \quad (15)$$

- Verifies if $V_{Sd_2} \leq V_{Rd}$;

2.3) Verification in phase 03 – Steel-concrete composite beam, $t=\infty$ and $n = \frac{3E_a}{E_c}$

- Loads: (1) + (2) + (3) + (4) + (5) + (6) + (7) + (8) + (9);
- Call routine 1 – Calculation of the ENA of the homogenized section for $t=\infty$ and $n = \frac{3E_a}{E_c}$;
- Calculation of forces due to concrete shrinkage (P9):

$$P_9 = \gamma_{g3} \cdot \frac{E_c}{3} \cdot \varepsilon_{cs,\infty} \cdot A_c \quad (16)$$

$\varepsilon_{cs,\infty}$ is the strain caused by shrinkage.

- Calculation of the design axial force (N_{Sd_3}) of phase 3:

$$N_{Sd_3} = N_{Sd_2} + P_9 \quad (17)$$

- Calculation of the design bending moment (M_{Sd_3}) of phase 3:

$$M_{Sd_3} = M_{Sd_2} + \gamma_{g3} \cdot P_9 \cdot \left(y_{tr}' - \frac{t_c}{2} \right) \tag{18}$$

- Flexo-compression verification:

$$\frac{N_{Sd3}}{N_{Rd}} + \frac{8 \cdot M_{Sd_3}}{9 \cdot M_{Rd_2}} \leq 1 \tag{19}$$

For simplification, it is assumed that only the steel profile resists axial forces. Also, the design resistance to bending of phase 3 is the same as in phase 2.

3) Call routine 9 – Calculation of deflection.

4) Design according to Nunziata [18]:

- Calls design routine 10 by verification of stresses.

3 EXPERIMENTAL VALIDATION

To validate the changes proposed to the formulations of ABNT NBR 8800: 2008 [13], two experiments on pre-tensioned prestressed composite beams were used, one tested by Ayyub et al. [2] and the other tested by Chen and Gu [10].

3.1 Experiment performed by Ayyub et al. [2]

The prestressed composite beam tested by Ayyub et al. [2], named *Specimen A*, Figure 2, consists of a simply supported element with a span length of 4.575 m, subjected to concentrated loads of equal magnitude applied at two symmetrical points in relation to midspan at a distance of 0.915 m from supports. The cross-section features a steel profile W360 x 45 with f_y equal to 345 MPa, a concrete slab with a thickness of 76mm and f_{cj} equal to 33.4 MPa defined by compressive tests of three specimens cured for 90 days. The slab presents a width of 915mm. Prestressing was performed via steel tendons of grade 150 DYWIDAG Threadbars of 16mm, with f_{pyk} of 910 MPa and f_{ptk} of 1100 MPa, at a distance of 57mm from the lower surface of the bottom flange of the steel profile, and a prestressing force of 98kN applied to each tendon.

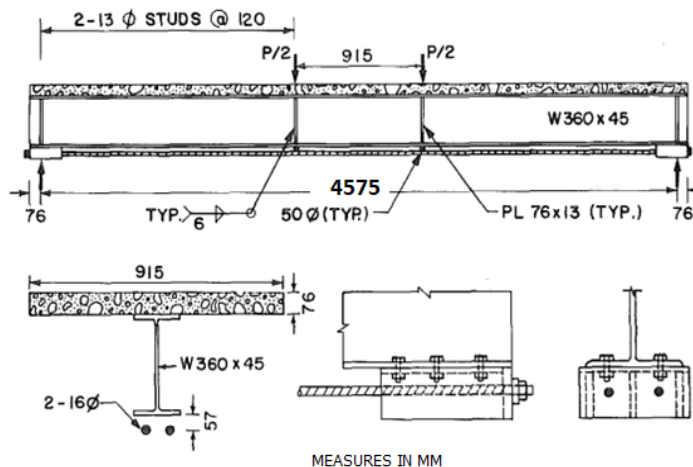


Figure 2. Test setup of the 4.575 m span prestressed steel-concrete composite beam. Source: Ayyub et al. [2].

Since prestressing was carried out before concreting the slab, increments in prestressing force were determined using the weight of fresh concrete and the experimental load, totaling an increase of 74.92 kN at the end of the test. Thus, the prestressing force at the moment of collapse is equal to 270.92 kN.

The ultimate limit state observed for the beam studied was the crushing of the concrete slab, which occurred for a bending moment of 586.51 kN.m. Calculating the characteristic resistance to bending moment according to the methodology proposed herein resulted in a value of 515.7 kN.m, 12.07% less than the ultimate load observed experimentally, showing that the proposed methodology favors structural safety.

3.2 Experiment performed by Chen and Gu [10]

The prestressed composite beam tested by Chen and Gu [10], named BS2, Figure 3, consists of a simply supported element with a span of 5 m, subjected to concentrated loads of equal magnitude applied at two symmetrical points in relation to midspan at a distance of 1.4 m from supports. The cross-section is composed using steel plates of 120 x 10 mm for the flanges and 250 x 6 mm for the web, with f_y equal to 367 MPa, a concrete slab with a thickness of 90 mm and f_{cj} equal to 30 MPa defined by compressive tests of three specimens cured for 30 days. The slab presents a width of 1100 mm. Prestressing was introduced by two steel tendons with a cross-sectional area of 137.4 mm², with f_{pyk} of 1680 MPa and f_{ptk} of 1860 MPa, at a distance of 30 mm from the lower surface of the bottom flange of the steel profile, and a prestressing force of 112.6 kN applied to each tendon.

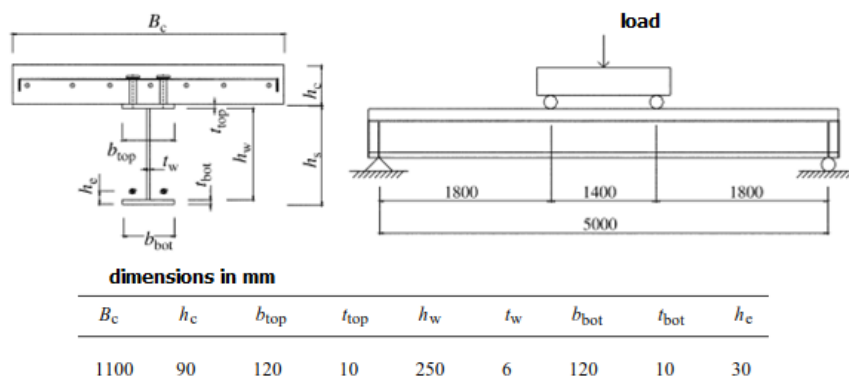


Figure 3. Test setup of the 5 m span prestressed steel-concrete composite beam. Source: Chen and Gu [10].

In this test, prestressing was carried out after concreting the slab, therefore only the test load was considered in the calculation of the prestressing force, totaling an increase of 72.1 kN at the end of the test, thus obtaining a prestressing force at collapse of 297.3 kN.

The ultimate limit state of the beam studied was the crushing of the concrete slab, which occurred for a bending moment of 373.2 kN.m. The characteristic resistance to bending moment, according to the methodology proposed herein, was 351.67 kN.m, therefore 5.77% less than the ultimate load verified experimentally, showing that the proposed methodology once again favors structural safety.

4 PARAMETRIC STUDY

4.1 Parametrization models

In the parametrized models, the composite beams analyzed feature double or monosymmetric steel profiles with smaller top flanges. The profiles are made of structural steel ASTM A572 gr. 50 (f_y equal to 345 MPa and f_u equal to 450 MPa). According to ABNT NBR 8800:2008 [13], monosymmetric cross-sections must meet the criteria given in Equations 20 and 21.

$$\frac{I}{9} \leq \alpha_y \leq 9 \text{ com } \alpha_y = \frac{I_{yc}}{I_{yt}} \tag{20}$$

$$A_{fs} + A_w > A_{fi} \tag{21}$$

where: I_{yc} is the moment of inertia of the compressed flange in relation to the axis that crosses the web at mid-thickness; I_{yt} is the moment of inertia of the tensioned flange in relation to the axis that crosses the web at mid-thickness; A_{fs} is the area of the upper flange, A_w is the area of the web and A_{fi} is the area of the bottom flange of the steel profile. In this study, the inverse of the coefficient α_y is called degree of monosymmetry, α_m , which may vary from 1 (for doubly symmetric sections) to a maximum value of 9.

$$\alpha_m = \frac{1}{\alpha_y} \text{ and } 1 \leq \alpha_m \leq 9 \tag{22}$$

To assess the influence of the degree of monosymmetry, profiles with the same cross-section area, equal to 178.00 cm², were selected. The weight of the steel I-beams is chosen as the same for all models on purpose, to allow an analysis of which geometric configuration provides the most resistant prestressed composite beam with the same cost. The height of the profiles was fixed at 550 mm, the thickness of the web at 12.50 mm and the width of the lower flange at 300 mm. The other parameters of the profiles were chosen to meet the specified steel area and provide variations in the degree of monosymmetry (α_m).

Values of beam length include 9, 10.5, 12, 13.5, 15 and 17 meters, consequently, the ratios between beam length and profile height studied are equal to approximately 16, 19, 22, 25, 27 and 31. The maximum free-span is 3.0 meters, equal to the distance between the beams perpendicular to the element under analysis. The distance of the beams adjacent to the beam studied is 5.0 meters.

Three eccentricity values (e_p) 630, 730 and 780 mm, were adopted for the beams as shown in Figure 4. For all models, the tendon path, formed by steel tendons CP-190 RB, is straight throughout the entire length of the beam.

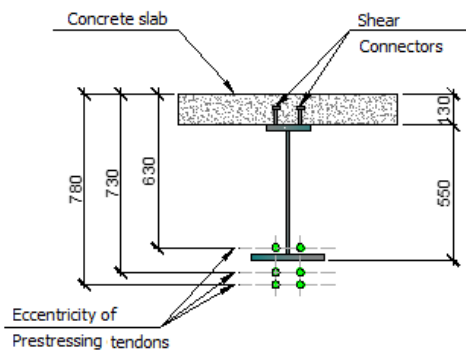


Figure 4. Profile scheme.

In total, one hundred and twenty composite steel and concrete beams were designed by the program, 90 of which are prestressed composite beams with eccentricity values of 630, 730 or 780mm. The remaining 30 models do not feature prestressing tendons. The models were named according to the presence or absence of prestressing using the acronyms VMP and VM, respectively. The prefixes VMP and VM are followed by the eccentricity values of prestressing tendons in relation to the top of the concrete slab, in turn followed by span length and the model number. Thus, the VMP 730x9x1 model indicates a prestressed composite beam with tendons located at 730mm from the top of the concrete slab, beam span equal to 9m and model number 1.

4.2 Methodology

Ultimate limit state verifications related to bending moment and shear force were performed along with checks of the serviceability limit state of excessive deformation. The verification of the interaction between axial and flexural forces was also performed. Tables 3 and 4 present the necessary checks for each of the aforementioned phases, considering the pre-tension method, that is, tendons are prestressed before casting the concrete slab.

Table 3. Design verifications of prestressed steel-concrete composite beam – ULS.

Verification phase	Loads	U.L.S Verification
1 st Phase: Steel Beam	q ₁ – Weight of the steel beam	- Compression ($N_{Sd1} \leq N_{Rd1}$);
	P – Prestressing force on tendons	- Bending Moment ($M_{Sd1} \leq M_{Rd1}$);
	q ₃ – Weight of the concrete slab	- Shear force ($V_{Sd1} \leq V_{Rd1}$);
	ΔP_4 - Increment of prestressing force due to concrete the weight of the concrete slab	- Flexure-compression Interaction
2 nd Phase: Prestressed steel-concrete composite beam t = 0	Including 1 st phase loads	
	q ₅ – Serviceability dead load	- Compression ($N_{Sd2} \leq N_{Rd2}$);
	q ₆ – Serviceability live load	- Bending Moment ($M_{Sd2} \leq M_{Rd2}$);
	ΔP_7 - Increment of prestressing force due to serviceability dead load	- Shear force ($V_{Sd2} \leq V_{Rd2}$);
$n = \frac{E_a}{E_c}$	ΔP_8 - Increment of prestressing force due to serviceability live load	- Flexure-compression Interaction
3 rd Phase: Prestressed steel-concrete composite beam t = ∞	Including 1 st and 2 nd phase loads	- Compression ($N_{Sd3} \leq N_{Rd3}$);
	q ₉ – Concrete slab shrinkage	- Bending Moment ($M_{Sd3} \leq M_{Rd3}$);
	$n = \frac{3E_a}{E_c}$	- Flexure-compression Interaction

Table 4. Verification phases of Prestressed steel-concrete composite beam – SLS.

Verification phase	1 st Fase: Steel Beam	2 nd Fase: Prestressed steel-concrete composite beam	
		t = 0 and $n = \frac{E_a}{E_c}$	t = ∞ and $n = \frac{3E_a}{E_c}$
Loads	q ₁ – Weight of the steel beam	q ₆ – Serviceability live load	q ₅ – Serviceability dead load
	P – Prestressing force on tendons	ΔP_8 - Increment of prestressing force due to serviceability live load	ΔP_7 - Increment of prestressing force due to serviceability dead load
	q ₃ – Weight of the concrete slab		
	ΔP_4 - - Increment of prestressing force due to the weight of the concrete slab		
Verifications S.L.S	Immediate deflection: (δ_1)	Short term deflection: (δ_2)	Long term deflection: (δ_3).
	Total deflection: $\delta_{total} = \delta_1 + \delta_2 + \delta_3 \leq L/350$		

To proceed with the analysis of the results, the values of applied and resistant bending moment are presented for the cross section at the middle of the beams, for phase 2. This is because these forces refer to the methodology from ABNT NBR 8800: 2008 [13] which does not address the effects of creep and shrinkage in ULS analyses, only in the calculation of deflection. The design stresses acting on the elements are presented for phase 3 because calculations are based on Nunziata [18], which considers the effects of shrinkage and creep in ULS verifications.

5 RESULT ANALYSIS

5.1 Influence of the ratio between span length and profile height

Regarding the flexural strength of composite beams without prestressing (VM), the analysis of the graph in Figure 5 allows us to observe that, when the L/d ratio goes from 16 to 31, there is an increase in the resistance to bending moment of 10.9% for doubly symmetric section and approximately 10.1% for the section with a degree of symmetry of 2.07 and approximately 9.0% for sections with a degree of symmetry of 2.83, 3.88 and 5.22. This increase in strength is a result of the increase in the effective width of the beam, in turn due to a larger span length.

In Figure 6, the composite steel and concrete beams without prestressing (VM) and the prestressed (VMP) with L/d ratio equal to approximately 31 did not meet the design criteria for flexural and axial interaction, since the utilization index (i_{a2}) was greater than 1. For L/d ratios of 16 to 25, the beams met the design criteria with clearance. As such, for the studied load type, it is noted that an L/d ratio equal to 27 would be the most advantageous in economic terms, since the utilization index (i_{a2}) was the closest to 1.

Regarding the flexural strength of prestressed beams (VMP), it is observed that the ultimate bending moment increases practically linearly as the L/d ratio increases from 16 to 27 for all degrees of monosymmetry. It is also observed that the beams with monosymmetric sections present the highest resistance to bending moment, reaching an increase of 35.6% when the L/d ratio grows from 16 to 27 for the sections with a monosymmetry index of 2.83, 3.88 and 5.22; 38.12% for the section with a degree of monosymmetry equal to 2.07 and 38.75% for the doubly symmetrical section. For values of L/d ratio equal to 27 and larger, the increase in resistance to bending moment is small for both monosymmetric sections (about 1%) and for the doubly symmetric section (about 3%).

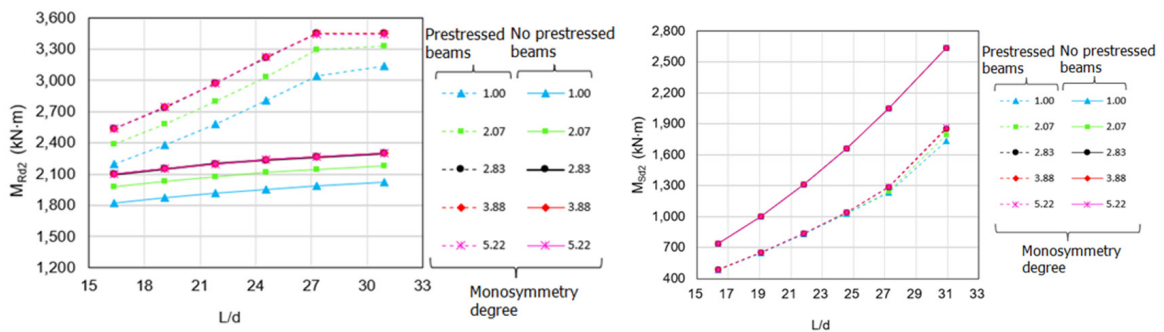


Figure 5. M_{Rd} and M_{Sd} versus L/d ratio graphs for $c_p = 730\text{mm}$.

The ratio between the resistance to bending moment of the prestressed composite beams and that of the unstressed composite beams, $M_{Rd2\ VMP} / M_{Rd2\ VM}$ shows that the ultimate bending moment of the prestressed composite beams is much higher than that of the composite beams without prestressing tendons; 21% and 55% greater for L/d ratios of 16 and 31, respectively in the case of doubly symmetrical section; and 21% and 49% higher for the L/d ratio equal to 16 and 31, respectively, in the case of the section with the highest monosymmetry degree. Larger spans have a higher $M_{Rd2\ VMP} / M_{Rd2\ VM}$ ratio because as the span increases, in addition to the increase in the effective width, the value of the prestressing force also increases, which contributes to a significant portion of the ultimate bending moment.

From Figure 5 it should be noted, as expected, that the bending moment acting on the prestressed composite beams is much lower than that of the conventional beams, being 35% and 34% lower for L/d ratios equal to 16 and 31 respectively for doubly symmetrical sections; and 34% and 29% higher for the L/d ratio equal to 16 and 31 respectively

for the section with the highest monosymmetry degree. The bending moment resulting from the application of the prestressing force reduces the bending moment acting on the prestressed composite beams. The ratio between the bending moment of the composite beams with prestressing and that of the composite beams without prestressing was almost constant, around 38%, which shows that prestressing considerably reduces bending effects regardless of span length.

Although prestressing presented considerable benefits, reducing the magnitude of bending moments and increasing flexural strength, improvements in beam utilization index (i_{a2}) is less evident, as seen in Figure 6, because the compression force on the profile due to the prestressing force introduces compression stresses that add to the stresses arising from bending. Significant improvements in the utilization index only occur for the doubly symmetrical section, for all L/d ratios. For sections with a lower degree of monosymmetry (2.07 and 2.83), the benefits of prestressing are only observed in smaller spans. In cross-sections with a higher degree of monosymmetry (3.88 and 5.22), prestressing was not advantageous, resulting in a lower utilization rate.

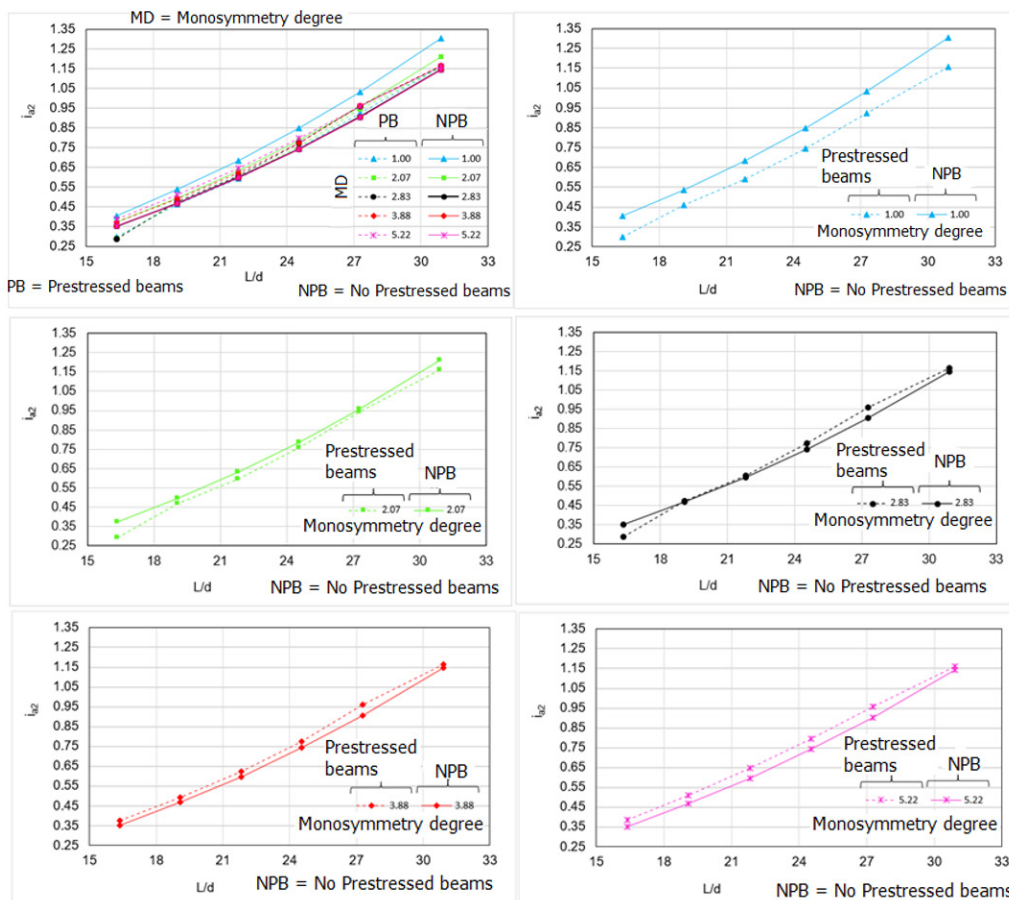


Figure 6. i_{a2} versus L/d ratio for $e_p = 730\text{mm}$.

If NBR 8800: 2008 [13] included the effects of shrinkage and creep in the calculation of design loads, there would be an average increase of approximately 4.1% to 10.7% for L/d ratios of 31 to 16, respectively. The ultimate bending moment of phase 3 is the same as that of phase 2.

5.2 Influence of the degree of monosymmetry

According to Figure 7, the composite beams without prestressing show an increase in the ultimate bending moment (M_{Rd2}) as the monosymmetry index (α_m) increases from 1.0 to 2.83 (on average 14.4%). Thereafter the resistance to

bending moment is practically constant. For each degree of monosymmetry, there is little difference between the values of flexural strength for the spans analyzed, with the beam with the largest span being the most resistant.

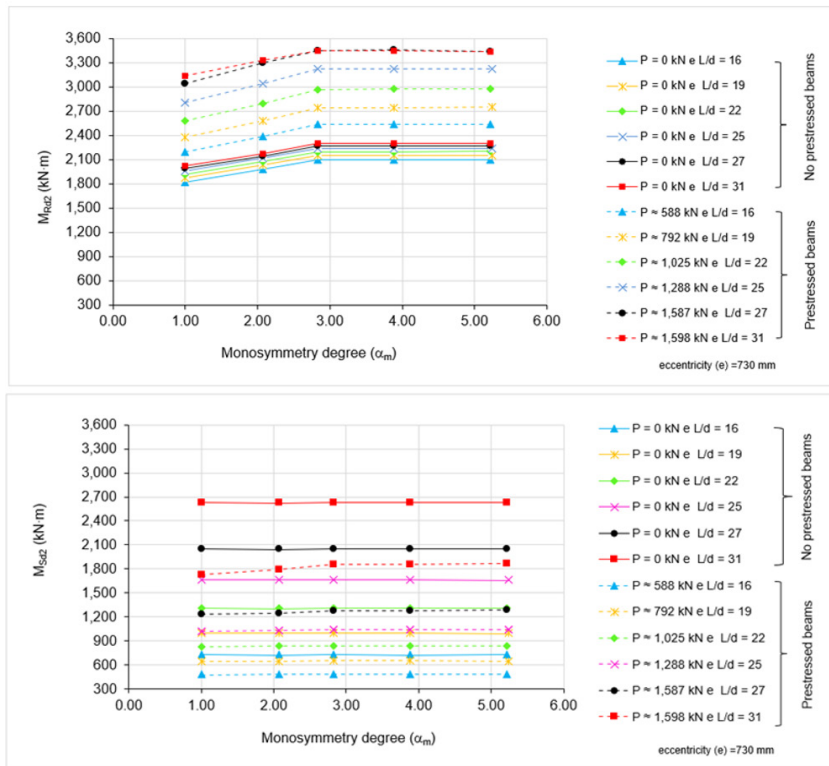


Figure 7. M_{Rd} and M_{Sd} versus monosymmetry degree graphs for $e_p = 730\text{mm}$.

It is observed that in the prestressed composite beams the ultimate moment also increases if the degree of monosymmetry is increased from 1.0 to 2.83 for all beams. There is an increase of approximately 15.4%, 15.1%, 14.9%, 14.8%, 13.3 and 10.0% in flexural strength for L/d ratios of 16, 19, 22, 25, 27 and 31, respectively. For monosymmetry index values larger than 2.83, the flexural strength is practically constant. For each monosymmetry index (α_m), there is a more noticeable difference between the values of flexural strength of the analyzed spans if compared to beams without pre-tension.

The second graph in Figure 7 illustrates the influence of monosymmetry index (α_m) on the value of the design bending moment (M_{Sd}) for an eccentricity (e_p) of 730mm. Composite beams without prestressing show no dependence between internal bending moment and the monosymmetry index (α_m). As for the prestressed composite beams, there is a slight dependence between the design bending moment and the monosymmetry index (α_m) when the latter varies from 1.0 to 2.83. There is a small increase of 2.2%, 2.7%, 0.37%, 0.40%, 2.3% and 9.3% in design bending moment for L/d ratios equal to 16, 19, 22, 25, 27 and 31, respectively, when the monosymmetry index increases from 1.0 to 2.83. This is a result of the prestressing force taking the properties of the cross section and the span length into account. For monosymmetry index values greater than 2.83, (from 2.83 to 5.22) variations in design load are small.

As shown in Figure 8, the use of monosymmetric profiles is only interesting from an economic point of view for composite beams without prestressing, in which a reduction in utilization rate is observed when the monosymmetry degree increases from 1.0 to 2.83.

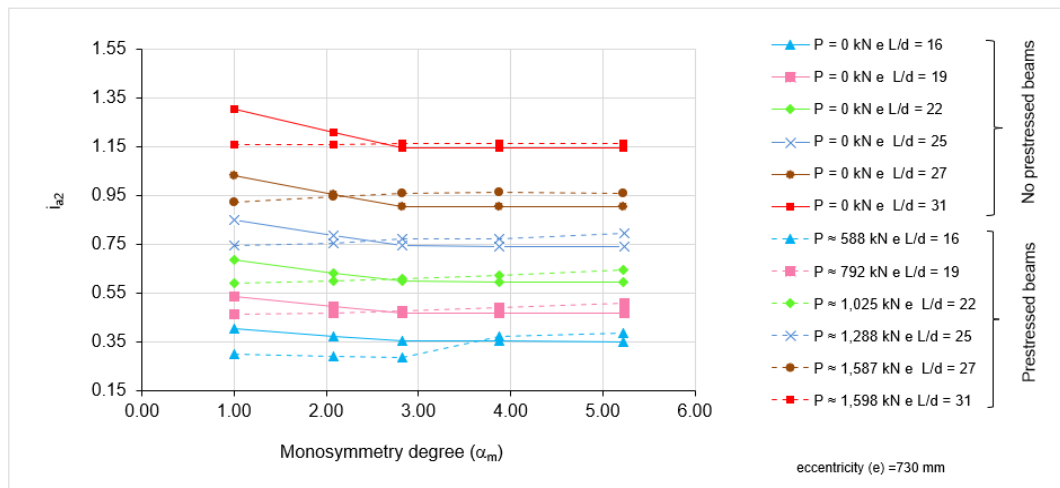


Figure 8. i_{a2} versus monosymmetry degree (α_m) graph for $e_p = 730$ mm.

5.3 Influence of eccentricity

Figures 9 to 14 present the influence of eccentricity (e_p) on the design resistance to bending moment (M_{Rd2}) of the prestressed beams for L/d ratios equal to 16, 19, 22, 25, 27 and 31, respectively.

Figure 9 indicates that, for an L/d ratio of 16, there are variations in flexural strength if (e_p) also varies, regardless of the degree of monosymmetry (α_m) of the beam. Regarding the smallest eccentricity value ($e_p = 630$ mm), the resistance to bending moment is reduced by an average of 5.20% when eccentricity increases 100 mm ($e_p = 730$ mm) and an average of 6.73% when eccentricity increases 150 mm ($e_p = 780$ mm) for all monosymmetry degree values (α_m).

Models		e_p (mm)	Ratio L/d	α_m	Prestressing Force (kN)	M_{Rd2} (kN)	$\frac{M_{Rd2} - M_{Rd2}(e_p=630)}{M_{Rd2}(e_p=630)}$ (%)	M_{Sd2} (kN)	$\frac{M_{Sd2} - M_{Sd2}(e_p=630)}{M_{Sd2}(e_p=630)}$ (%)	
	41	VMP _{630x9x41}	630	16	1.00	802.30	2,288.86	-	474.31	-
	1	VMP _{730x9x1}	730			533.15	2,195.59	-4.08%	482.00	1.62%
	21	VMP _{780x9x21}	780			452.36	2,165.75	-5.38%	485.69	2.40%
	42	VMP _{630x9x42}	630	16	2.07	912.62	2,509.54	-	476.62	-
	2	VMP _{730x9x2}	730			581.39	2,386.94	-4.89%	484.46	1.64%
	22	VMP _{780x9x22}	780			487.26	2,350.05	-6.36%	488.17	2.42%
	43	VMP _{630x9x43}	630	16	2.83	1,015.67	2,688.19	-	478.68	-
	3	VMP _{730x9x3}	730			622.06	2,534.66	-5.71%	486.75	1.69%
	23	VMP _{780x9x23}	780			515.70	2,490.95	-7.34%	490.49	2.47%
	44	VMP _{630x9x44}	630	16	3.88	1,018.43	2,688.38	-	478.41	-
	4	VMP _{730x9x4}	730			623.71	2,535.54	-5.69%	486.35	1.66%
	24	VMP _{780x9x24}	780			517.09	2,492.00	-7.30%	490.03	2.43%
	45	VMP _{630x9x45}	630	16	5.22	1,021.85	2,688.81	-	478.00	-
	5	VMP _{730x9x5}	730			626.17	2,536.99	-5.65%	485.63	1.60%
	25	VMP _{780x9x25}	780			519.35	2,493.74	-7.26%	489.17	2.34%

Figure 9. Eccentricity influence - L/d ratio = 16.

The design bending moment is slightly influenced by eccentricity. For the smallest value of eccentricity, ($e_p = 630\text{mm}$), the design bending moment increases an average of 1.64% when eccentricity increases 100 mm ($e_p = 730$ mm) and 2.41% when eccentricity increases 150 mm ($e_p = 780$ mm).

Figures 10, 11 and 12 show that the L/d ratios equal to 19, 22 and 25 present a behavior similar to that of the models with L/d ratios of 16, regarding variations in flexural strength as a function of eccentricity. For the lowest eccentricity value ($e_p = 630\text{mm}$), the ultimate bending moment decreases by an average of 9.09% (Figure 10), 7.66% (Figure 11) and 6.72% (Figure 12) when the eccentricity increases 100 mm ($e_p = 730$ mm) and decreases on average 10.92% (Figure 10), 9.91% (Figure 11) and 9.39% (Figure 12) when the eccentricity increases 150 mm ($e_p = 780$ mm).

Models		e_p (mm)	Ratio L/d	α_m	Prestressing Force (kN)	M_{Rd2} (kN)	$\frac{M_{Rd2} - M_{Rd2}(e_p=630)}{M_{Rd2}(e_p=630)}$ (%)	M_{Sd2} (kN)	$\frac{M_{Sd2} - M_{Sd2}(e_p=630)}{M_{Sd2}(e_p=630)}$ (%)	
	111	VMP _{630x10.5x111}	630	19	1.00	1,081.36	2,506.88	-	636.80	-
	101	VMP _{730x10.5x101}	730			718.72	2,380.19	-5.05%	646.55	1.53%
	106	VMP _{780x10.5x106}	780			609.86	2,339.62	-6.67%	651.14	2.25%
	112	VMP _{630x10.5x112}	630	19	2.07	1,229.24	2,750.54	-	640.34	-
	102	VMP _{730x10.5x102}	730			783.09	2,583.93	-6.06%	650.64	1.61%
	107	VMP _{780x10.5x107}	780			656.29	2,533.74	-7.88%	655.34	2.34%
	113	VMP _{630x10.5x113}	630	19	2.83	1,368.05	3,100.27	-	635.20	-
	103	VMP _{730x10.5x103}	730			837.85	2,741.76	-11.56%	653.98	2.96%
	108	VMP _{780x10.5x108}	780			694.57	2,682.31	-13.48%	658.78	3.71%
	114	VMP _{630x10.5x114}	630	19	3.88	1,371.79	3,098.90	-	634.92	-
	104	VMP _{730x10.5x104}	730			840.09	2,743.96	-11.45%	653.40	2.91%
	109	VMP _{780x10.5x109}	780			696.46	2,684.64	-13.37%	658.12	3.65%
	115	VMP _{630x10.5x115}	630	19	5.22	1,376.97	3,097.42	-	634.49	-
	105	VMP _{730x10.5x105}	730			843.61	2,747.16	-11.31%	652.38	2.82%
	110	VMP _{780x10.5x110}	780			699.66	2,688.10	-13.21%	656.90	3.53%

Figure 10. Eccentricity influence - L/d ratio = 19.

Once again, the internal moment suffers little influence from the eccentricity. In relation to the lower eccentricity value ($e_p = 630\text{mm}$), the design bending moment increases on average 2.37% (Figure 10) and 1.6% (Figure 11) and decreases on average 2.0% (Figure 12) when the eccentricity increases by 100 mm ($e_p = 730$ mm). When the eccentricity increases by 150 mm ($e_p = 780$ mm), the design bending moment increases on average 3.1% (Figure 10), 2.28% (Figure 11) and decreases on average 1.39% (Figure 12).

In short, for L/d ratios equal to 16, 19, 22 and 25, the eccentricity of 630 mm provides the greatest flexural strength for all degrees of monosymmetry and, also, the lowest bending moment in most cases, thus this eccentricity would be ideal for designs featuring the aforementioned L/d ratios.

Models			e_p (mm)	Ratio L/d	α_m	Prestressing Force (kN)	M_{Rd2} (kN)	$\frac{M_{Rd2} - M_{Rd2}(e_p=630)}{M_{Rd2}(e_p=630)}$ (%)	M_{Sd2} (kN)	$\frac{M_{Sd2} - M_{Sd2}(e_p=630)}{M_{Sd2}(e_p=630)}$ (%)
	46	VMP _{630x12x46}	630	22	1.00	1,402.70	2,748.78	-	817.21	-
	6	VMP _{730x12x6}	730			932.77	2,583.52	-6.01%	828.88	1.43%
	26	VMP _{780x12x26}	780			791.64	2,530.55	-7.94%	834.23	2.08%
	47	VMP _{630x12x47}	630	22	2.07	1,592.80	3,018.02	-	822.59	-
	7	VMP _{730x12x7}	730			1,014.90	2,800.60	-7.20%	835.49	1.57%
	27	VMP _{780x12x27}	780			850.62	2,734.98	-9.38%	841.15	2.26%
	48	VMP _{630x12x48}	630	22	2.83	1,772.51	3,241.83	-	826.15	-
	8	VMP _{730x12x8}	730			1,085.74	2,969.99	-8.39%	840.21	1.70%
	28	VMP _{780x12x28}	780			900.12	2,892.33	-10.78%	846.08	2.41%
	49	VMP _{630x12x49}	630	22	3.88	1,776.57	3,244.15	-	825.82	-
	9	VMP _{730x12x9}	730			1,087.93	2,972.77	-8.37%	839.71	1.68%
	29	VMP _{780x12x29}	780			901.90	2,895.15	-10.76%	845.51	2.38%
	50	VMP _{630x12x50}	630	22	5.22	1,782.59	3,247.61	-	825.00	-
	10	VMP _{730x12x10}	730			1,092.25	2,977.22	-8.33%	838.32	1.62%
	30	VMP _{780x12x30}	780			905.87	2,899.83	-10.71%	843.86	2.29%

Figure 11. Eccentricity influence - L/d ratio = 22.

Models			e_p (mm)	Ratio L/d	α_m	Prestressing Force (kN)	M_{Rd2} (kN)	$\frac{M_{Rd2} - M_{Rd2}(e_p=630)}{M_{Rd2}(e_p=630)}$ (%)	M_{Sd2} (kN)	$\frac{M_{Sd2} - M_{Sd2}(e_p=630)}{M_{Sd2}(e_p=630)}$ (%)
	91	VMP _{630x13.5x91}	630	25	1.00	1,765.94	3,014.63	-	1,013.11	-
	81	VMP _{730x13.5x81}	730			1,175.01	2,805.65	-6.93%	1,026.46	1.32%
	86	VMP _{780x13.5x86}	780			997.46	2,738.56	-9.16%	1,032.39	1.90%
	92	VMP _{630x13.5x92}	630	25	2.07	1,994.87	3,307.42	-	1,023.49	-
	82	VMP _{730x13.5x82}	730			1,278.27	3,038.28	-8.14%	1,035.75	1.20%
	87	VMP _{780x13.5x87}	780			1,071.63	2,955.11	-10.65%	1,042.20	1.83%
	93	VMP _{630x13.5x93}	630	25	2.83	2,036.95	3,451.35	-	1,079.00	-
	83	VMP _{730x13.5x83}	730			1,367.48	3,220.94	-6.68%	1,042.13	-3.42%
	88	VMP _{780x13.5x88}	780			1,133.97	3,122.56	-9.53%	1,048.94	-2.79%
	94	VMP _{630x13.5x94}	630	25	3.88	2,035.75	3,451.37	-	1,080.21	-
	84	VMP _{730x13.5x84}	730			1,368.19	3,223.03	-6.62%	1,042.37	-3.50%
	89	VMP _{780x13.5x89}	780			1,134.31	3,124.54	-9.47%	1,049.20	-2.87%
	95	VMP _{630x13.5x95}	630	25	5.22	1,958.26	3,407.24	-	1,102.96	-
	85	VMP _{730x13.5x85}	730			1,372.98	3,228.21	-5.25%	1,040.96	-5.62%
	90	VMP _{780x13.5x90}	780			1,138.63	3,129.80	-8.14%	1,047.48	-5.03%

Figure 12. Eccentricity influence - L/d ratio = 25.

Figures 13 and 14, for L/d ratios equal to 27 and 31, respectively, show a quite different behavior from that observed in L/d ratios equal to 16, 19, 22 and 25. There is no significant variation of ultimate bending moment when eccentricity value changes. More specifically, for the L/d ratio equal to 27, Figure 13, the ultimate bending moment is reducing on average 0.62% when the eccentricity increases by 100 mm ($e_p = 730$ mm) and 3.07% when the eccentricity increases by 150 mm ($e_p = 780$ mm). The design moment is reduced with the eccentricity, varying from - 7.89% to -12.37% when the eccentricity increases by 100 mm ($e_p = 630$ mm to $e_p = 730$ mm), in similar fashion to when the eccentricity increases by 150 mm ($e_p = 630$ mm for $e_p = 780$ mm), showing reductions of about -7.43% to -14.14%.

Models			e_p (mm)	Ratio L/d	α_m	Prestressing Force (kN)	M_{Rd2} (kN)	$\frac{M_{Rd2} - M_{Rd2}(e_p=630)}{M_{Rd2}(e_p=630)}$ (%)	M_{Sd2} (kN)	$\frac{M_{Sd2} - M_{Sd2}(e_p=630)}{M_{Sd2}(e_p=630)}$ (%)
	51	VMP _{630x15x51}	630	27	1.00	1,847.12	3,113.36	-	1,342.33	-
	11	VMP _{730x15x11}	730			1,445.82	3,047.02	-2.13%	1,236.36	-7.89%
	31	VMP _{780x15x31}	780			1,227.68	2,963.39	-4.82%	1,242.62	-7.43%
	52	VMP _{630x15x52}	630	27	2.07	1,922.03	3,316.90	-	1,407.31	-
	12	VMP _{730x15x12}	730			1,572.66	3,296.90	-0.60%	1,249.01	-11.25%
	32	VMP _{780x15x32}	780			1,318.81	3,193.72	-3.71%	1,256.04	-10.75%
	53	VMP _{630x15x53}	630	27	2.83	1,957.63	3,457.32	-	1,464.25	-
	13	VMP _{730x15x13}	730			1,626.08	3,454.36	-0.09%	1,283.20	-12.37%
	33	VMP _{780x15x33}	780			1,395.54	3,372.72	-2.45%	1,265.01	-13.61%
	54	VMP _{630x15x54}	630	27	3.88	1,956.12	3,458.04	-	1,465.54	-
	14	VMP _{730x15x14}	730			1,624.61	3,455.06	-0.09%	1,284.52	-12.35%
	34	VMP _{780x15x34}	780			1,395.98	3,374.82	-2.41%	1,265.29	-13.66%
	55	VMP _{630x15x55}	630	27	5.22	1,934.32	3,447.03	-	1,472.79	-
	15	VMP _{730x15x15}	730			1,601.18	3,440.36	-0.19%	1,295.93	-12.01%
	35	VMP _{780x15x35}	780			1,398.30	3,378.61	-1.98%	1,264.57	-14.14%

Figure 13. Eccentricity influence - L/d ratio = 27.

For the L/d ratio equal to 31, Figure 14, in relation to the lowest eccentricity value ($e_p = 630\text{mm}$), the design resistance to bending moment increases on average 0.27% when the eccentricity increases 100 mm ($e_p = 730\text{ mm}$) and increases by an average of 2.94% when the eccentricity increases by 150 mm ($e_p = 780\text{ mm}$). The design bending moment decreases on average 9.30% when the eccentricity increases by 100 mm ($e_p = 730\text{ mm}$) and decreases on average 5.81% when the eccentricity increases by 150 mm ($e_p = 780\text{ mm}$).

Models			e_p (mm)	Ratio L/d	α_m	Prestressing Force (kN)	M_{Rd2} (kN)	$\frac{M_{Rd2} - M_{Rd2}(e_p=630)}{M_{Rd2}(e_p=630)}$ (%)	M_{Sd2} (kN)	$\frac{M_{Sd2} - M_{Sd2}(e_p=630)}{M_{Sd2}(e_p=630)}$ (%)
	56	VMP _{630x17x56}	630	31	1.00	1,750.83	3,116.60	-	1,916.80	-
	16	VMP _{730x17x16}	730			1,496.04	3,138.89	0.72%	1,734.57	-9.51%
	36	VMP _{780x17x36}	780			1,839.60	3,450.97	10.73%	2,045.06	6.69%
	57	VMP _{630x17x57}	630	31	2.07	1,815.04	3,314.92	-	1,984.71	-
	17	VMP _{730x17x17}	730			1,537.29	3,328.42	0.41%	1,796.81	-9.47%
	37	VMP _{780x17x37}	780			1,819.66	3,440.89	3.80%	2,052.11	3.40%
	58	VMP _{630x17x58}	630	31	2.83	1,841.53	3,450.38	-	2,043.66	-
	18	VMP _{730x17x18}	730			1,545.17	3,453.59	0.09%	1,854.32	-9.26%
	38	VMP _{780x17x38}	780			1,430.10	3,454.32	0.11%	1,774.28	-13.18%
	59	VMP _{630x17x59}	630	31	3.88	1,839.60	3,450.97	-	2,045.06	-
	19	VMP _{730x17x19}	730			1,543.42	3,454.06	0.09%	1,855.78	-9.26%
	39	VMP _{780x17x39}	780			1,428.42	3,454.75	0.11%	1,775.76	-13.17%
	60	VMP _{630x17x60}	630	31	5.22	1,819.66	3,440.89	-	2,052.11	-
	20	VMP _{730x17x20}	730			1,521.80	3,440.26	-0.02%	1,866.94	-9.02%
	40	VMP _{780x17x40}	780			1,406.68	3,439.50	-0.04%	1,788.89	-12.83%

Figure 14. Eccentricity influence - L/d ratio = 31.

In summary, it is concluded that a more comprehensive analysis is necessary to determine the ideal value of design eccentricity for prestressed composite beams, since the flexural behavior, in terms of resistant and applied bending moment, differs in relation to eccentricity changes according to the selected L/d ratio. It is important to note that, in the methodology used herein, the variation in the eccentricity of the tendon implies a variation in the value of the initial prestressing force, according to the flexo-compression interaction equation (Equation 5). Therefore, an increase in eccentricity does not always cause an increase in bending resistance, since the initial prestressing force is reduced to meet the conditions given in Equation 5.

5.4 Analysis of stresses

The stresses were determined considering the interaction of axial forces and bending moment for phase 3, according to the methodology of Nunziata [18].

Figure 15 shows that the design stresses on the upper flange of the steel profile are smaller than the design yield stress of steel ($f_{yd} = 31.4 \text{ kN/cm}^2$) in all models studied, except for the composite beams without prestressing with an L/d ratio equal to 31 and prestressed composite beams with an L/d ratio equal to 31 and eccentricity of 630 mm. The composite beams without prestressing present compressive stresses on the upper flange that are considerably larger than the values observed for prestressed composite beams. It is also observed that the variation in the eccentricity (e_p) of the tendon influences the stress distribution on the upper flange of the steel profile. For this graph, the models with eccentricity of 780 mm and doubly symmetrical section presented the lowest stress values.

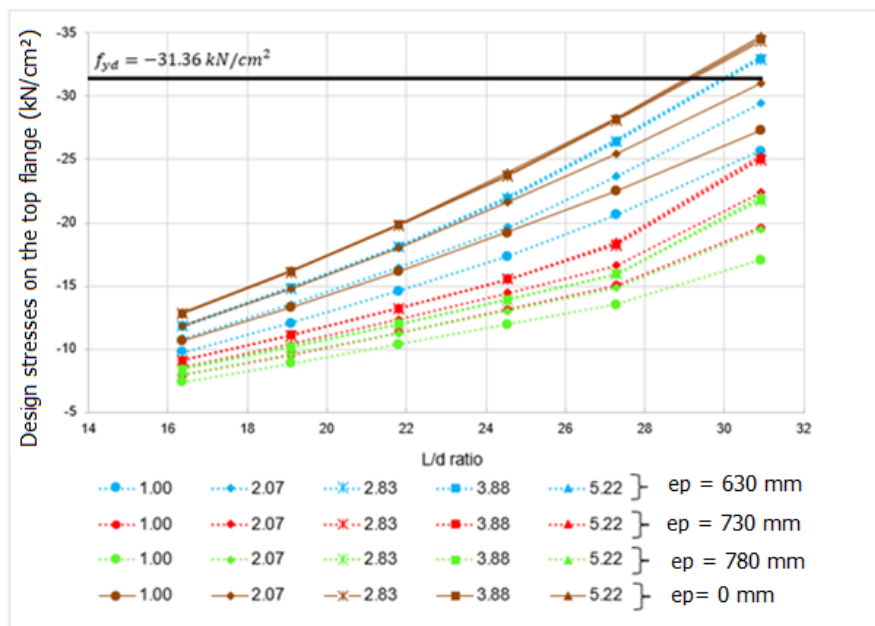


Figure 15. Graph of design stresses on the top flange of the profile.

From the graph in Figure 16, regarding the stresses on the bottom flange of the steel profile, it is noted that the models of composite beams without prestressing do not meet criteria for the design yield stress of steel, except for the models with an L/d ratio equal to 16 and in some models with an L/d ratio of 19. Thus, many of the beams without prestressing that do not pass the Nunziata methodology [18] meet the criteria of ABNT NBR 8800: 2008 [13]. This is due to the former being more conservative since it considers the beginning of yield at a point on the cross-section as the failure criteria, while the criteria of ABNT NBR 8800: 2008 [13] considers the plastic hinge formation as the ULS.

Still concerning stresses on the lower flange of the steel profile, most of the prestressed composite beams meet the criterion for yield stress limits, except for models with an L/d ratio equal to 31. According to the graph presented in ABNT NBR 8800: 2008 [13], the models with eccentricity of 680 mm and monosymmetry indexes equal to 2.83; 3.88 and 5.22 present the smallest stresses.

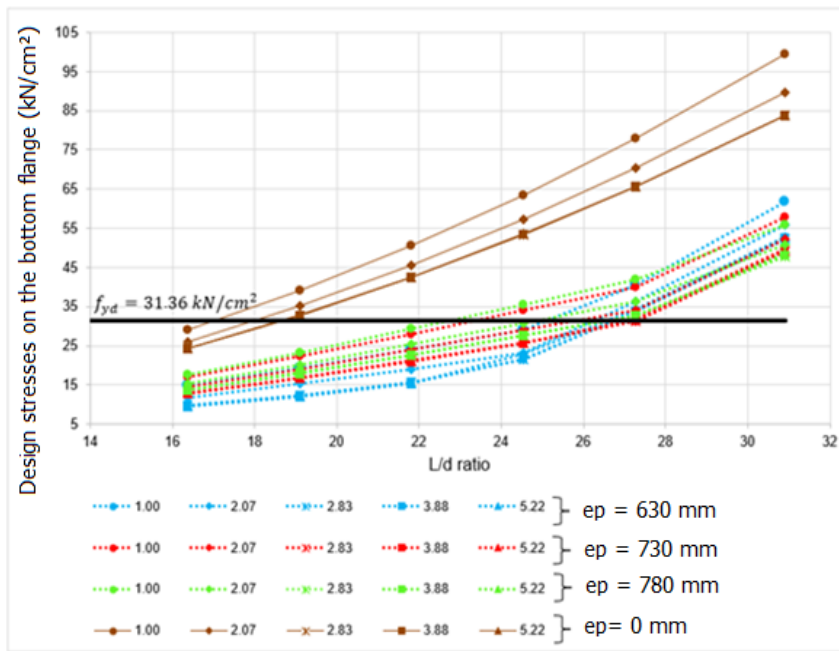


Figure 16. Graph of design stresses on the bottom flange of the profile.

Figure 17 shows the normal design stress on the top surface of the concrete slab as a function of the L/d ratio. It is observed that the design stress on the concrete portion of the models without prestressing is less than that of prestressed composite beams. No case exceeded the ultimate stress of $0.85f_{cd}$, equal to $1.51 \text{ kN} / \text{cm}^2$. Input data used to calculate each model is given in Table 3.

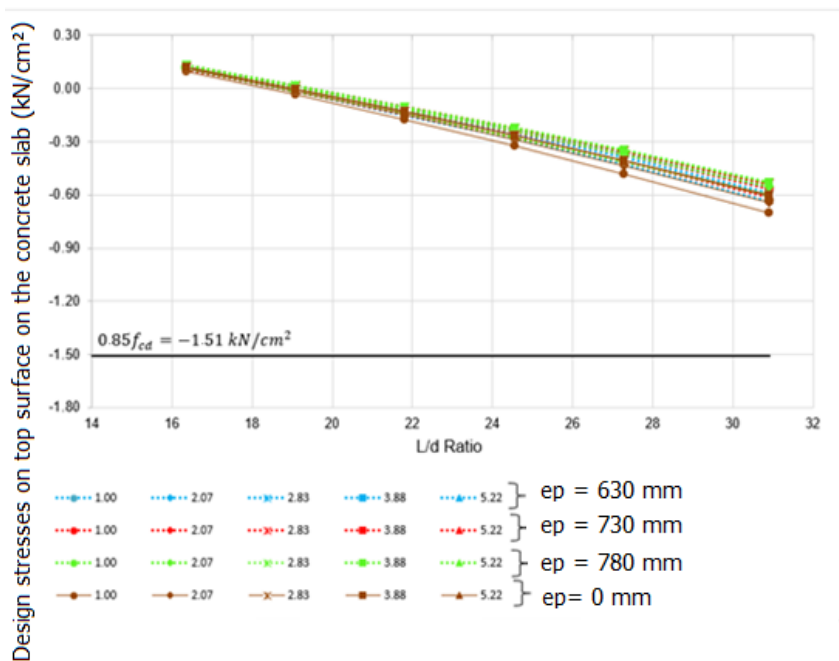


Figure 17. Graph of stresses on the top surface of the concrete slab.

5.5 Analysis of displacements

The maximum deflection of the prestressed composite beams and of composite beams without prestressing was determined by homogenizing the composite section according to the computer routine from which the displacements at midspan are obtained. Figure 18 shows the maximum deflection value of the beams for different L/d ratios.

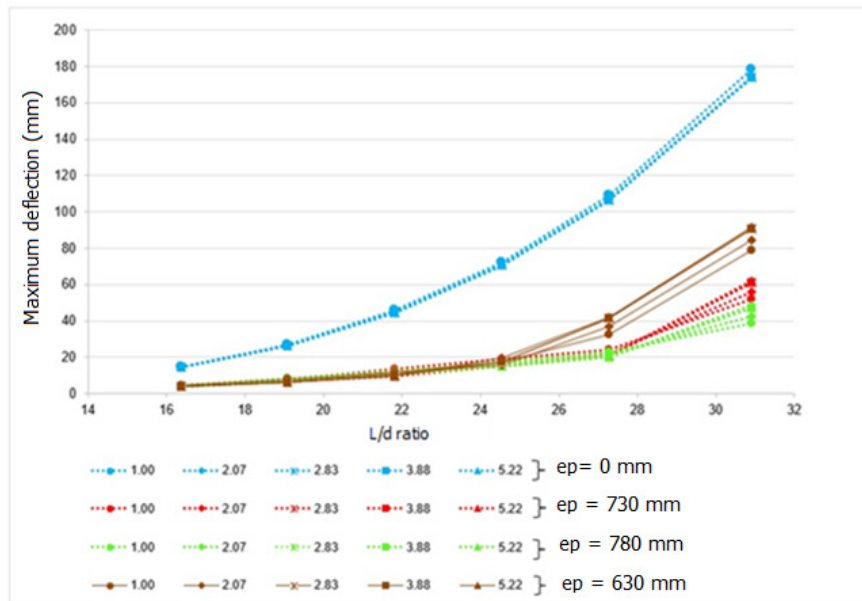


Figure 18. Maximum deflection of the beams at midspan.

It is noted that prestressing has a significant influence on the Serviceability Limit State of excessive deformation when analyzing the reduction of the midspan deflection of the prestressed composite beam in relation to the non-prestressed composite beams, percentage-wise $[(d_{VM} - d_{VMP})/d_{VM}, (\%)]$. According to Figure 18, for an L/d ratio of 31 and eccentricity of 630 mm, the midspan deflection of the prestressed composite beam ($d_{VMP} = 78.92$ mm) is less than half the value found for the composite beam without prestressing ($d_{VM} = 178.42$ mm), with a reduction of 56%. The midspan deflection reduction reaches 72% for an L/d ratio of 19 and eccentricity of 630 mm, where the deflection is reduced from 27.16 mm to 7.69 mm.

It is also noted that for L/d ratios smaller than 25, there is no significant change in the midspan deflection of prestressed beams when the eccentricity value is changed. For L/d ratios equal to 27 and 31, however, higher values of eccentricity of the prestressing force presented smaller displacements. A deflection reduction percentage of 34% is achieved between eccentricity values of 730mm and 630mm and 25% between the eccentricities of 730mm and 780 mm.

In summary, the analysis of results allowed an assessment of the benefits of applying external prestressing in composite beams for controlling both ULS and SLS, since there was an increase in strength and stiffness of the beams.

6 CONCLUSION

The main objective of this research was to study the behavior of composite steel and concrete beams with external prestressing using the pre-tensioning technique with straight tendons. A computer program was developed to calculate design forces and design cross-sections as regions of positive bending moment of the beams following two design methodologies: one based on ABNT NBR 8800: 2008 [13] and the other according to Nunziata [18]. In both methodologies, the prestressing strength is estimated according to Nunziata [18]. The program checks safety conditions for Ultimate Limit States and the Serviceability Limit State of excessive deformation.

A parametric study, using the computer program developed, was implemented in 120 composite steel and concrete beams of different characteristics, 90 of them with external prestressing and 30 of them without prestressing. The influence of the following parameters was evaluated: ratio between the length of the beam and the height of the steel

profile; monosymmetry degree of the steel profile and eccentricity of the prestressing force. The latter was restricted to two different locations for prestressing tendons, above and below the bottom flange of the steel profile.

Results indicate that the composite beams of steel and concrete without prestressing (VM) and prestressed (VMP) with an L/d ratio of approximately 31 do not meet the combined bending-compression design criteria for the load applied, 5 kN/m² of live load, since the utilization rate was larger than 1. For L/d ratios ranging from 16 to 25, the beams meet the design criteria with clearance. It should be noted that the L/d ratio equal to 27 would be the most advantageous in economic terms since the utilization rate was the closest to 1.

Although prestressing has generated a considerable improvement in the behavior of the composite beams under bending, reducing the design bending moment and increasing the ultimate bending moment, its improvement in the rate of utilization of the beam was less noticeable, because the compression force on the steel profile due to the prestressing force introduces compressive stresses that are added to stresses arising from bending. Significant improvements in the utilization index only occur for the doubly symmetrical section. For sections with a lower monosymmetry (2.07 and 2.83), the beneficial effects of prestressing are only observed in smaller spans. In cross-sections with a higher monosymmetry degree (3.88 and 5.22), prestressing is not advantageous, resulting in smaller utilization rates when compared to beams without prestressing.

It was also concluded that the use of monosymmetric profiles in composite beams is only interesting from an economic point of view for beams without prestressing a with monosymmetry index smaller than 2.83.

For the three cases of tendon eccentricity (630, 730 and 780 mm) studied, it was observed, for L/d ratios equal to 16, 19, 22 and 25, that the 630 mm eccentricity provides the greatest flexural strength and the smallest design bending moment, so this eccentricity would be ideal for the design. For L/d ratios equal to 27 and 31, it was not possible to establish the ideal design eccentricity, since the eccentricity that provides the largest bending resistance also provides the highest value of design bending moment.

Finally, it is observed that prestressing has a significant influence on the control of the SLS of excessive displacement when analyzing reductions in deflection at the midspan of prestressed composite beams in relation to unstressed composite beams. The result analysis allowed the observation of the benefits of applying external prestressing in composite beams for controlling ULS and SLS, since there was an increase in both strength and stiffness of the beams.

Although underutilized in Brazil due to little knowledge of the system and its design methods, it is clear that prestressed composite steel and concrete beams have great relevance for maintenance projects, recovery of existing structures and design of large new structures. International scientific literature presents theoretical and experimental studies aimed at understanding the structural behavior of this type of beam, and this research contributed to a greater understanding of design methodologies for these structural elements.

ACKNOWLEDGEMENTS

The authors would like to acknowledge the Foundation for Support of Research and Innovation of Espírito Santo (FAPES) for the support during the development of this research.

REFERENCES

- [1] M. S. Troitsky, *Prestressed Steel Bridges: Theory and Design*. 16th ed. New York, USA: Van Nostrand Reinhold, 1990.
- [2] B. M. Ayyub, Y. G. Sohn, and H. Saadatmanesh, "Prestressed composite girders under positive moment," *J. Struct. Eng.*, vol. 116, no. 11, pp. 2931–2951, 1990. [http://dx.doi.org/10.1061/\(ASCE\)0733-9445\(1990\)116:11\(2931\)](http://dx.doi.org/10.1061/(ASCE)0733-9445(1990)116:11(2931)).
- [3] R. Szilard, "Design of prestressed composite steel structures," *J. Struct. Div.*, vol. 85, no. 9, pp. 97–123, 1959.
- [4] P. G. Hoadley, "Behavior of prestressed composite steel beams," *J. Struct. Div.*, vol. 89, no. 3, pp. 21–34, 1963.
- [5] J. C. Strass "An experimental and analytical study of prestressed composite beams," M.S thesis, Rice Univ., Houston, TX, 1964.
- [6] R. S. Regan, "An analytical study of the behavior of prestressed composite beams," M.S thesis, Rice Univ., Houston, TX, 1966.
- [7] H. Saadatmanesh, P. Albrecht, and B. M. Ayyub, "Analytical study of prestressed composite beams," *J. Struct Eng.*, v. 115, n. 9, p. 2364–2381, 1989. [https://doi.org/10.1061/\(ASCE\)0733-9445\(1989\)115:9\(2364\)](https://doi.org/10.1061/(ASCE)0733-9445(1989)115:9(2364)).
- [8] H. Saadatmanesh, P. Albrecht, and B. M. Ayyub, "Guidelines for flexural design of prestressed composite beams," *J. Struct Eng.*, v. 115, n. 11, p. 2944–2961, 1989. [https://doi.org/10.1061/\(ASCE\)0733-9445\(1989\)115:11\(2944\)](https://doi.org/10.1061/(ASCE)0733-9445(1989)115:11(2944)).
- [9] H. Saadatmanesh, P. Albrecht, and B. M. Ayyub, "Experimental study of prestressed composite beams," *J. Struct Eng.*, v. 115, n. 9, p. 2348–2363, 1989. [https://doi.org/10.1061/\(ASCE\)0733-9445\(1989\)115:9\(2348\)](https://doi.org/10.1061/(ASCE)0733-9445(1989)115:9(2348)).

- [10] S. Chen and P. Gu, "Load carrying capacity of composite beams prestressed with external tendons under positive moment," *J. Construct. Steel Res.*, vol. 61, pp. 515–530, 2005. <http://dx.doi.org/10.1016/j.jcsr.2004.09.004>.
- [11] A. C. H. Nelsen, "Comportamento estrutural de beams mistas de aço and concreto com protensão externa," M.S. thesis, Centr. Ciênc. Exat. Tec., Univ. Fed. São Carlos, São Carlos, SP, 2013.
- [12] B. T. Linhares "Análise de pontes em estruturas mistas de aço-concreto de seção caixão com protensão externa," M.S thesis, Dep. Eng. Civil, Univ. Fed. Rio Grd. Sul, Porto Alegre, RS, 2015.
- [13] Associação Brasileira de Normas Técnicas, *Projeto de Estrutura de Aço e de Estrutura Mista de Aço e Concreto de Edifícios*, ABNT NBR 8800:2008, 2008.
- [14] T. Lou, S. M. R. Lopes, and A. V. Lopes, "Numerical modeling of externally prestressed steel-concrete composite beams," *J. Construct. Steel Res.*, vol. 61, pp. 226–236, 2016. <http://dx.doi.org/10.1016/j.jcsr.2016.02.008>.
- [15] R. T. Liban and N. Tayşi, "Nonlinear finite element analysis of composite cantilever beam with external prestressing," *Int. J. Civ. Environ. Eng.*, vol. 11, no. 4, pp. 511–517, 2017., <http://dx.doi.org/10.5281/zenodo.1130935>.
- [16] Microsoft, "Microsoft Office Excel," USA: Microsoft Corporation, 2013.
- [17] Microsoft, "Microsoft Visual Basic Express," USA: Microsoft Corporation, 2013.
- [18] V. Nunziata, *Strutture in Acciaio Precompresso*, 2nd ed. Palermo, Italy: Dario Flaccovio, 2004.
- [19] Associação Brasileira de Normas Técnicas, *Projeto de Estruturas de Concreto – Procedimento*, ABNT NBR 6118:2014, 2014.
- [20] Associação Brasileira de Normas Técnicas, *Fios de Aço para Concreto Protendido – Especificação*, ABNT NBR 7482:2008, 2008
- [21] Associação Brasileira de Normas Técnicas, *Cordoalhas de Aço para Estruturas de Concreto Protendido – Especificação*, ABNT NBR 7483:2008, 2008
- [22] K. D. Ribeiro, "Análise and dimensionamento de beams mistas de aço and concreto com protensão externa," M.S thesis, Dep. Eng. Civ., Univ. Fed. Esp. Sto., Vitória, ES, 2018.

Author contributions: KDR: conceptualization, funding acquisition, methodology, writing; TTT: conceptualization, experimental proof, methodology, writing; LARL and AFGC: supervision, formal analysis.

Editors: Maurício de Pina Ferreira, José Luiz Antunes de Oliveira e Sousa, Guilherme Aris Parsekian.